A Carrier-Arraying Demonstration at Goldstone for Receiving Pioneer 11 Signals

T. T. Pham, M. K. Simon, and T. K. Peng
Telecommunications Systems Section

M. H. Brockman[1]

S. S. Kent[2]

R. Weller[3]

A carrier-arraying technique was demonstrated at Goldstone in May 1990. The Block III receivers of two 34-m antennas, DSS 12 and DSS 15, were arrayed together to receive S-band (2.3-GHz) signals from the Pioneer 11 spacecraft. Carrier phases in the two receivers were synchronized by the analog phase-lock loops, and carrier signals were added at an intermediate frequency to enhance tracking performance. The receiver at DSS 15, which had been unable to lock up and track the Pioneer 11 signal by itself due to a wider tracking loop bandwidth and a higher system temperature, was now able to track the carrier and produce usable baseband signals. The receiver at DSS 12 achieved a reduction of the rms phase error, increasing the telemetry symbol SNR by an average of 0.35 dB. The baseband signals from both antennas were then synchronized and combined using the existing Baseband Assembly, thereby achieving a total symbol SNR increase of 2.5 ± 0.7 dB relative to DSS 12 alone. Baseband combining would have been impossible without carrier arraying in this case. In analyzing the performance of carrier arraying, previous models only treated the rms phase errors caused by the ground receiver thermal noises. But as very narrow tracking loops were employed, the contribution of phase noises transmitted from the spacecraft or generated in the ground-receiver oscillators should be included. In this article, a more comprehensive model is presented to permit evaluation of both thermal and phase-noise effects. The analysis agrees well with observed data.

[1] Consultant, M. H. Brockman and Associates.

[2] Consultant, Mainstream Engineering.

[3] CDI Consultants.

I. Introduction

The Deep Space Network (DSN) has the capability to combine baseband signals from several antennas by using the Baseband Assembly (BBA). Baseband combining depends on baseband signals to be demodulated at each antenna, which requires the receiver at each antenna to be in lock. Some distant spacecraft, such as Pioneer 10 and 11, have signal levels so low that only the 70-m antenna with the narrowest (3-Hz bandwidth) receiver tracking loop can track these signals with adequate performance, as shown in Table 1. As of May 1990, the 34-m standard (STD) antenna could receive these signals using a 3-Hz loop, with unsteady performance. However, the 34-m high-efficiency antenna (high efficiency at 8.4 GHz but not at 2.3 GHz) was unable to acquire or track the signals at all because of its higher system temperature and wider loop bandwidth.

The technique described in this article, as depicted conceptually in Fig. 1, enabled both of the 34-m antennas to lock onto the weak carrier signals and produce baseband signals in an engineering demonstration conducted at Goldstone, California. The local oscillator signal of DSS 12, a 34-m STD antenna station, was sent to DSS 15, a 34-m high-efficiency (HEF) antenna station, to aid carrier acquisition and tracking there. Since the Doppler frequency difference between the two stations was small (less than ± 6 Hz), a very narrow loop could be used at DSS 15 to track the carrier. The carrier signal from DSS 15 was then sent at an intermediate frequency (IF) to DSS 12 to be combined with the carrier signal at DSS 12. Receiver performance at both antennas was improved.

The general term *carrier arraying* is used to refer to both carrier-aiding and carrier-combining operations. In this demonstration, carrier aiding enabled DSS 15 to acquire and track the spacecraft signal. Carrier combining further improved tracking performance at DSS 12 and DSS 15.

This carrier-arraying technique was first suggested in [1]. The performance was analyzed in detail in [2], including the effects of thermal noises from the ground stations. Specific design parameters for antennas with different gain/temperature (G/T) ratios were suggested in [3]. Hardware modules implementing this technique were first installed in the receiver development laboratory at JPL and tested in January 1990. The same modules were then installed at DSS 12 and DSS 15 in April 1990 for field testing. Pioneer 11 telemetry signals were successfully received by the system on May 3 and 6, 1990.

Section II describes the configuration of the carrier array system used in the demonstration. Section III describes the data received from the spacecraft and discusses the observed effects of carrier arraying on receiver performance. Section IV includes a comparison of actual data with the calculation of an enhanced mathematical model. This model, given in detail in Appendix A, permits evaluation of both thermal noise and phase-noise effects. Section V includes the conclusions. Appendix B includes an analysis of the optimal choice of weighting factors for carrier combining. Also given are the equations from the existing phase-lock-loop and carrier-arraying theories relevant to this study.

II. System Description

A. Configuration

A detailed block diagram of the modified Block III receivers at DSS 12 and DSS 15 is given in Fig. 2. The modification includes modified or new hardware modules for carrier arraying and three fiber-optic lines connecting the two receivers: the 70-MHz local oscillator (LO) from DSS 12 to DSS 15, the 10-MHz IF signal from DSS 15 to DSS 12, and the 100-MHz frequency reference from DSS 15 to DSS 12. A series of switches was used to allow the receivers to operate in either "normal" or "carrier array" mode, identified as "N" or "A" in Fig. 2. Normal mode permits the receiver to provide regular flight support without using the array modules.

During the demonstration, the first LO into the S-band mixer at DSS 15 was always aided by the DSS 12 LO signal. The DSS 15 carrier was combined with the DSS 12 carrier at 10-MHz IF by a switch at DSS 12. The combiner was switched in and out several times to measure the effect of carrier combining.

At DSS 12, the downlink signal was first amplified by the maser low-noise amplifier, with a system noise temperature around 20 K at zenith. The signal was downconverted with a reference signal coming from the carrier tracking loop. The output at 50 MHz was further downconverted to 10 MHz. One of the 10-MHz IF distribution amplifier outputs was used for baseband demodulation. The other 10-MHz IF signal passed through a 550-Hz predetection filter into the carrier tracking loop. This filtered 10-MHz IF signal could be combined with a similar signal from DSS 15 by the action of the carrier combiner switch. The power levels of the two combining carriers were kept relatively constant by the automatic gain control (AGC) in the Block III receivers. The 70-MHz LO signal from this carrier tracking loop was distributed to DSS 15 to drive its first local oscillator.

At DSS 15, the received S-band signal was first amplified by the high-electron-mobility transistor (HEMT) low-noise amplifier with a noise temperature around 35 K at zenith. It was then mixed with the reference signal originating from DSS 12, producing a 50-MHz IF at the S-band mixer output. The 50-MHz signal was again mixed with a 60-MHz signal from the phase-locked loop to produce a 10-MHz IF. This IF signal was further converted to baseband. A separate branch of this signal was filtered through a 4950-Hz predetection filter, and subsequently a much narrower filter, for carrier tracking. The 10-MHz IF signal after the 4950-Hz filter was also distributed to DSS 12 for carrier combining.

Primary modifications to the existing Block III receivers for carrier arraying included the following:

1. The 3-Hz Tracking Loop at DSS 12. The carrier tracking loop had a threshold loop bandwidth ($2B_{LO}$) of 3 Hz and a loop damping factor (r_0) of 4. This loop bandwidth was narrow enough to provide sufficient carrier signal-to-noise ratio in the loop and large enough to track the carrier in the presence of Doppler uncertainty without aiding.

2. The 0.13-Hz Tracking Loop at DSS 15. Since the operating noise temperature at DSS 15 was higher than that at DSS 12, a narrower tracking loop with a threshold loop bandwidth ($2B_{LO}$) of 0.13 Hz was used to reduce the phase error due to thermal noise. Such a narrow loop was adequate to track the carrier signal because it only had to track the Doppler frequency difference between the two antennas. Most of the Doppler frequency shift due to Earth rotation was tracked out by the 3-Hz loop of the DSS 12 receiver through the common 70-MHz LO.

3. Common Frequency Reference Between DSS 12 and DSS 15. The receivers at DSS 12 and DSS 15 shared the same source of reference frequency through a fiber-optic link. This common reference eliminated any potential phase drift between the two IF signals to be combined and any apparent Doppler in the DSS 15 receiver due to a drifting 70-MHz LO.

4. Gain Modification To Reduce the Interference of Spurious Signals. When an initial attempt was made at DSS 15 to acquire the low-level Pioneer carrier signals, spurious signals of significant power relative to the carrier were detected. One spurious signal adjacent to the 50-MHz IF interfered with the signal acquisition. A 20-dB amplifier had to be installed upstream from the mixer to reduce the spurious signal effect to an acceptable level. As carrier arraying is only needed when the signal level is near the thermal noise threshold, low-level spurious signals that have no adverse effect on other occasions can actually interfere with the signal reception in this case. This experience highlighted the need for careful testing of spurious signals before committing the new system to flight support.

B. Operational Procedure

Prior to the tracking, the telemetry detector phase was adjusted to remove any bias. The carrier combiner was adjusted to align the phases of the two signals and set the weighting factors for combining. The factors were set to unity in this demonstration. Later analysis, given in Appendix B, indicated that a different choice of weighting factors could have been used to optimize the signal-to-noise ratio in the tracking loop at DSS 12. That choice would have increased the carrier tracking loop SNR (P_c/N_0B_L) by 0.13 dB.

Because of the narrow tracking loop employed, it was not possible for DSS 15 to acquire the signal independently. The acquisition process always started with the receiver at DSS 12. After phase lock, DSS 12 sent its first LO to DSS 15. The DSS 15 receiver was then tuned to compensate for the frequency difference between the two stations, allowing the DSS 15 receiver to acquire the signal. Carrier combining was ready to be activated after both stations established lock.

III. Data Received From the Spacecraft

A. Results

1. May 3, 1990. Figure 3 presents the symbol SNR (ST_s/N_0) of the carrier-arrayed and baseband-combined telemetry measured on May 3. The telemetry rate was 16 bits per sec convolutionally coded, or 32 symbols per sec modulated on a 32-kHz subcarrier. Each data point in Fig. 3, and later in Figs. 4(a) and 5, represents measurements at the interval of 60 sec. At all times, the DSS 15 receiver was carrier-aided from DSS 12. Carrier combining was activated in periods 8:45–9:30 GMT and 10:00–10:15 GMT and was deactivated from 9:30–10:00 GMT. Only the performance of the DSS 12/DSS 15 baseband-combined telemetry was directly measured. DSS 12 or DSS 15 telemetry symbol SNR could not be individually measured due to equipment constraints. During this period, the system operated in a 3-way mode with uplink signals transmitted from DSS 61, a 34-m antenna in Madrid, Spain. The system noise temperature at zenith

was recorded as 21.2 K at DSS 12 and 35.4 K at DSS 15. However, the effective noise temperature was 3 K higher since the signals were received in the elevation range of 42–46 deg.

On this date, the DSS 14 station also tracked Pioneer 11 spacecraft and its measured symbol SNR is presented in Fig. 4(a). A drop of 0.3 dB was observed from 1-way to 3-way operation.

Normally the received carrier signal level is measured with the AGC signal provided by the receiver. This measurement was not made at DSS 12 because the receiver gain was changed and was not calibrated due to lack of time. Instead, the carrier signal level at DSS 12 was inferred from the -166.2 ± 0.3-dBm level measured at DSS 14, as shown in Fig. 4(b). Since the receiving antenna gains are known to differ by 7.3 ± 0.3 dB,[4] the carrier power at DSS 12 was estimated to be -173.5 ± 0.4 dBm. All uncertainties are referenced to 1σ.

2. May 6, 1990. A more comprehensive set of measurements was made, as shown in Fig. 5. The DSS 12 telemetry and the baseband-combined DSS 12/DSS 15 telemetry were individually measured, and 1-way and 3-way telemetry data were both available. Carrier combining was activated and deactivated many times to observe its effects.

The system noise temperatures at zenith were 25.6 K at DSS 12 and 36.5 K at DSS 15 (an increase in the noise temperature at DSS 12 was a result of the microwave switches having been configured in a diplexed mode, as compared with the nondiplexed configuration on May 3). For the elevation range in which data were taken, i.e., 21–47 deg, the effective noise temperature at DSS 12 was 32.1–28.6 K at DSS 12 and 43.0–39.5 K at DSS 15. In the 1-way mode, the track started with receiver carriers combined from 6:45–8:15 GMT. Carrier combining was turned off in the next 15 minutes from 8:15–8:30. At 8:35, the spacecraft signals changed to 3-way mode. In the next one and a half hours, the carrier-combining option was again activated twice from 9:00–9:45 and 10:00–10:15.

Note that the symbol SNR dropped by 0.2 to 0.3 dB when the spacecraft signal changed from 1-way to 3-way mode as a result of transponder uplink noise. Note also that the baseband-combined data in the 3-way mode on May 6 were about 0.9 dB lower than the data on May 3. This was caused by the difference in the system noise temperature (0.8-dB difference at 40-deg elevation) on two different passes.

3. Statistical Analysis of Received Data. In analyzing the data, a least-squared-fitting algorithm that included the known elevation-angle dependence on antenna gain and system temperature was used to generate best-estimate curves. Any measurement of telemetry symbol SNR was modeled as the input symbol SNR minus a degradation in the receiver, minus another degradation in the subcarrier demodulation and symbol synchronization process, plus a baseband-combining gain, if appropriate. The input symbol SNR was determined from the measured carrier power, a known modulation index, and a known functional dependence on elevation angle. The degradation in subcarrier demodulation and symbol synchronization was assumed to be 0.8 dB when the Subcarrier Demodulator Assembly/Symbol Synchronizer Assembly (SDA/SSA) was used and 0.3 dB when the BBA was used.[5] The baseband-combining gain reflected the algebraic sum of the symbol SNRs of the two baseband signals, assuming that the two signals were optimally combined [4]. The algorithm solved the receiver degradation as an unknown constant in the least-squared sense, thus defining the curve.

Only data collected under the same configuration (1-way versus 3-way, carrier-combined versus noncombined, single-station versus baseband-combined) were fitted together as an ensemble. The results of these fittings are the curves given in Figs. 3, 4(a), and 5.

B. Discussions

1. Effect of Carrier Arraying on DSS 15 Performance. The 70-MHz local oscillator from DSS 12 enabled the DSS 15 receiver to acquire and track the carrier signal and demodulate the telemetry baseband. Symbol SNR of the DSS 15 telemetry was not measured directly. However, it could be inferred from the DSS 12 telemetry symbol SNR and the known difference in system temperature. After using this inferred value to calculate the symbol SNR of the baseband-combined telemetry of DSS 12 and DSS 15, the estimate agreed with the measurement to within 0.2 dB.

2. Effect of Carrier Combining on the DSS 12 Telemetry. In the stand-alone mode, DSS 12 performed very close to the prediction. For example, the measured symbol SNR was 0.1 dB at 8:15 GMT on May 6 (Fig. 5),

[4] *Deep Space Network/Flight Project Interface Design Handbook*, 810-5, Rev. D, vol. 1, modules TCI-10 and TCI-30 (internal document), Jet Propulsion Laboratory, Pasadena, California, June 1, 1990.

[5] Ibid., module TLM-30.

while the predicted value was 0.3 dB based on G/T and the estimated symbol SNR degradation in the system. When the carriers were combined, the symbol SNR at DSS 12 increased by 0.35±0.5 dB (Fig. 5 or Table 4, 3-way mode). This is consistent with the estimated 0.4-dB improvement based on a model given in Section IV below.

3. Effect of Carrier Arraying and Baseband Combining Together. Carrier arraying enabled DSS 15 to lock up the receiver and produce telemetry baseband signals. Baseband combining added DSS 12 and DSS 15 signals together, resulting in an observed 2.15 ± 0.5-dB increase in symbol SNR relative to DSS 12 telemetry (Table 4, 1-way). Given the G/T ratios of both antennas and the estimated comparable degradations in both systems, this baseband-combining gain is consistent with expectations.

4. Telemetry Degradation When the Spacecraft Downlink Changes From 1-Way to 3-Way Mode. The 0.2–0.3-dB degradation observed in Fig. 5 is not surprising since the phase noise generated on the spacecraft downlink due to thermal noise on the uplink contributed an additional amount of phase error in the ground receiver carrier tracking loop. This phenomenon, which was also observed independently at DSS 14, is explained in [5].

IV. Performance of Data Compared With Analytical Model

A. An Improved Mathematical Model for Carrier Arraying

Since telemetry degradation in the carrier demodulation process depends on the mean-squared value of the total phase error that appears at the output of the phase detector, every source of carrier phase error contributes to telemetry degradation. Existing mathematical models only address the contribution of the thermal noise referring to the front end of the ground receiver [2]. Yet, it is known that phase noises contained in the received spacecraft signal and phase noises generated in the ground receiver (normally in the voltage-controlled oscillator [VCO]) also contribute to the phase error. In the months following the demonstration, the mathematical model given in [2] was extended to take into account phase noises generated on the spacecraft and in the receiver VCO. This extended model is described in detail in Appendix A. Application of the model to the specific array environments at DSS 12 and DSS 15 is explained below.

1. Mean-Squared Phase Error in the First Receiver (DSS 12). For a two-receiver system, the mean-squared phase error observed in the main receiver (DSS 12) in an array configuration can be expressed as

$$\sigma^2_{\phi_1} = \frac{1}{2\pi j}\int \left|\frac{H_1(s)}{1+H_1(s)[1-H_2(s)](G-1)}\right|^2 ds \frac{N_{01}}{2P_1\cos^2\theta_m} + \frac{1}{2\pi j}\int \left|\frac{H_1(s)[1-H_2(s)]}{1+H_1(s)[1-H_2(s)](G-1)}\right|^2 ds \frac{N_{02}}{2P_2\cos^2\theta_m}$$

$$+ \frac{1}{2\pi j}\int \left|\frac{1-H_1(s)}{1+H_1(s)[1-H_2(s)](G-1)}\right|^2 S_{\Delta\psi 1}(s)ds + \frac{1}{2\pi j}\int \left|\frac{H_1(s)[1-H_2(s)]}{1+H_1(s)[1-H_2(s)](G-1)}\right|^2 S_{\psi R2}(s)ds \quad (1)$$

where

$H_1(s)$ = the closed-loop transfer function of the DSS 12 receiver

$H_2(s)$ = the closed-loop transfer function of the DSS 15 receiver

P_1, P_2 = the total received power at DSS 12 and DSS 15, respectively

N_{01}, N_{02} = thermal noise spectral densities of DSS 12 and DSS 15

θ_m = the telemetry modulation index

$S_{\Delta\psi 1}$ = the noise spectral density of the spacecraft phase noise and the DSS 12 receiver VCO phase noise (independent sources)

$S_{\psi R2}$ = the noise spectral density of the DSS 15 receiver phase noise

This equation is taken from Eq. (A-15) of Appendix A with two antennas ($N = 2$), unity carrier combining weighting factor ($\beta = 1$), and the same amplitude of car-

rier signals ($\gamma = 1$). As a result, the carrier-array gain G, as defined in Eq. (A-16), equals 2 when the carriers are combined and 1 when the carriers are not combined.

The first term in Eq. (1) is the contribution of thermal noise from DSS 12. The second term is the thermal noise contribution from the DSS 15 receiver to the DSS 12 receiver through carrier combining at IF. Spacecraft phase noise and DSS 12 VCO phase-noise contribution are seen in the third term. The fourth term describes the contribution of the DSS 15 receiver phase noise, which affects DSS 12 through carrier combining.

Notice that the effects of the spacecraft and VCO phase noise are filtered with a high-pass function $[1 - H(s)]$, whereas thermal noise is filtered through a low-pass function $H(s)$. Since the phase-noise spectral density at the VCO output is often modeled as $1/f^3$, careful consideration needs to be given to the choice of loop bandwidth. The lower the loop bandwidth, the more contribution can be expected from the VCO. If the VCO or spacecraft phase noise dominates, a tracking loop of larger bandwidth is better. On the other hand, a narrower loop is desirable if thermal noise becomes dominant.

When the 10-MHz IF from DSS 15 is not combined with that of DSS 12, the second and fourth terms become zero and the factor G becomes unity. The equation then reduces to the well-known phase error expression for a single receiver.

2. Mean-Squared Phase Error in the Second Receiver (DSS 15). Similarly, the phase error in the second receiver at DSS 15 is summarized in the following equation:

$$\sigma^2_{\phi_2} = \frac{1}{2\pi j}\int \left|\frac{H_1(s)[1-H_2(s)]}{1+H_1(s)[1-H_2(s)](G-1)}\right|^2 ds \frac{N_{01}}{2P_1\cos^2\theta_m} + \frac{1}{2\pi j}\int \left|\frac{H_1(s)[1-H_2(s)](G-1)+H_2(s)}{1+H_1(s)[1-H_2(s)](G-1)}\right|^2 ds \frac{N_{02}}{2P_2\cos^2\theta_m}$$

$$+ \frac{1}{2\pi j}\int \left|\frac{[1-H_1(s)][1-H_2(s)]}{1+H_1(s)[1-H_2(s)](G-1)}\right|^2 S_{\Delta\psi 1}(s)\,ds + \frac{1}{2\pi j}\int \left|\frac{[1-H_2(s)]}{1+H_1(s)[1-H_2(s)](G-1)}\right|^2 S_{\psi R2}(s)\,ds \tag{2}$$

where all parameters are defined as in Eq. (1).

This equation is taken from Eq. (A-25) in Appendix A. The first term is the thermal noise coming from the DSS 12 receiver through the first LO. The second term consists of two parts, both caused by thermal noise in the DSS 15 receiver itself. The first part, $H_1(s)[1 - H_2(s)]$, passes the receiver thermal noise from DSS 15 to DSS 12 via carrier combiner and then back to the DSS 15 through the first LO. The second portion, $H_2(s)$, is the well-known effect of the thermal noise from the DSS 15 front end to the DSS 15 receiver itself. The third term represents the phase-noise contribution from the spacecraft and DSS 12 VCO through the first LO. The DSS 15 receiver VCO phase-noise contribution is shown in the last term.

B. Predicted Phase Errors in the 1-Way Mode

This model was used to estimate the mean-squared phase errors in both receivers for this demonstration. The phase-noise spectral density from the spacecraft oscillator is assumed to vary as c/f^3, where f is the frequency offset from the carrier, and c is a coefficient that depends on the phase-noise characteristics of the VCO and the frequency multiplier following it. The value of c for Pioneer 10, a similar spacecraft, was previously determined from measurements to be approximately $4\pi \times 10^{-4}$ [6]. The coefficient for the Block III receiver VCO, with a frequency multiplier of 96 as used at DSS 12, was determined to be 4.4×10^{-3} in [7]. The coefficient for the DSS 15 receiver was much smaller because of a smaller frequency multiplier of 3, instead of 96, used for the carrier-arraying tracking loop. The value of c for the receiver at DSS 15 was therefore reduced by a factor of $(3/96)^2$ to 4.3×10^{-6}. The carrier-to-noise density ratio (P_c/N_0) used in the calculation reflected the actual condition during the demonstration. The calculated mean-squared phase errors contributed by all sources at the DSS 12 receiver are given in Table 2.

Several comments can be offered. First, the thermal noise effect of the DSS 12 receiver was reduced in the

carrier-combined mode because of the presence of a limiter. Specifically, as the 10-MHz IF signal from DSS 15 was injected into the carrier combiner at DSS 12, noise of the 4950-Hz bandwidth from DSS 15 came with it. This resulted in a higher suppression of signal power and, in effect, the loop gain and loop bandwidth were reduced, as reflected in Eqs. (A-18) and (A-19). Secondly, the transfer function $H_1(f)[1 - H_2(f)]$ for the thermal noise of the DSS 15 receiver has effectively the same bandwidth as that of $H_1(f)$, making the DSS 15 thermal noise equally important as that of DSS 12. Thirdly, the contribution from the spacecraft oscillator turned out to be relatively small, because the oscillator phase-noise density decreases sharply with frequency, as $1/f^3$. Its effect on the phase error depends on $1 - H_1(f)$, which is a high-pass filter, attenuating all but an insignificant portion of the oscillator spectrum. This high-pass filter also limits the contribution of the DSS 12 VCO noise, which also varies as c/f^3. The contribution of the DSS 15 VCO phase noise was estimated to be small due to the small frequency multiplier following the VCO.

To estimate the symbol SNR degradation due to the root-mean-squared phase errors in the receiver, the statistical average of $\cos^2 \phi$ was used:

$$\text{Symbol SNR degradation} = < \cos^2 \phi > \qquad (3)$$

where ϕ represents the phase errors discussed above, with zero mean and a standard deviation equal to the total root-mean-squared error given in Table 2. By using this formula, the symbol SNR degradations can be estimated with and without carrier combining, as given in Table 2.

As for the DSS 15 receiver, similar calculations were made based on Eq. (A-25) of Appendix A. The results are presented in Table 3. Estimated degradations are also given.

C. Predicted Phase Errors in the 3-Way Mode

In the 3-way mode, the estimates given in Table 2 remain the same except for the spacecraft phase-noise contribution. In this case, the spacecraft phase noise was dominated by the effect of the transponder thermal noise in the uplink. The bandwidth of the phase-noise power spectrum was equal to that of the spacecraft carrier tracking loop, with one-sided bandwidth B_L of 54 Hz ($2B_{L0} = 21$ Hz at threshold), much larger than the ground receiver loop bandwidth. More precisely, the two-sided phase spectral density at the ground receiver input was $0.5\,K^2|H_{sc}(f)|^2 N_{osc}/P_{csc}$, where $H_{sc}(f)$ was the closed-loop transfer function of the spacecraft receiver, K was the downlink to uplink frequency ratio (240/221), N_{osc} was the spacecraft noise temperature (1039 K), and P_{csc} was the uplink carrier signal level received at the spacecraft (−135.5 dBm on May 3 and May 6, 1990). The spacecraft employed a predetection filter of 1900 Hz. By using these parameters in the third term of Eqs. (1) and (2), the phase error contributed by the uplink thermal noise is estimated to be 0.19 rad in either receiver, as noted at the bottom of Tables 2 and 3. This contribution caused an additional loss of −0.14 dB in both receivers.

D. Comparison Between Model and Observed Data

Table 4 provides a summary of the discussions above. The actual and expected performances under different conditions are compared. The discrepancies are within 0.2 dB in most conditions. Two inconsistencies are apparent in Table 4:

(1) The observed baseband-combining gain in the 3-way mode was significantly lower than the 1-way mode (1.4 versus 2.1 dB) or the prediction (2.3 dB). The phase noise coming down from the spacecraft, as caused by the uplink thermal noise, may have affected baseband-combining efficiency in a way not yet understood. Traditional calculation of baseband-combining optimal gain assumes the signals from different antennas to be correlated and noises to be uncorrelated. In this case, that assumption may not be valid because the noises received by these antennas from the same spacecraft were not necessarily uncorrelated. The more pronounced impact of correlated noise in a 3-way mode was likely caused by a wider noise spectrum of the spacecraft-tracking loop, as compared with the narrow $1/f^3$ spectrum in the 1-way mode. The effect of correlated noise from the spacecraft or the propagation media on baseband combining needs further investigation.

(2) Measurements conducted in the laboratory at JPL prior to the Goldstone demonstration showed a larger carrier-combining gain than had been predicted, as seen in Table 4. In the laboratory, two independent receiver channels with independent thermal noise sources and fiber-optic links were used to simulate conditions at DSS 12 and DSS 15. The baseband signal, from a single receiver or a resistive baseband combiner, was sent to the Compatibility Test Area (CTA21) for detection. The laboratory tests differed from the field demonstration in two respects: (a) Doppler was not simulated, the signal frequency was fixed throughout the test, and (b) no phase noise was introduced in the input carrier signal, only white Gaussian thermal noise was added. These two effects, however, did not explain the

0.9-dB difference in Table 4. This test was not repeated because the carrier-arraying modules had been removed from the receiver, which was needed for other purposes. It is suggested that the next carrier array experiment should examine the difference, if any, between laboratory test results and the analytical prediction of a model such as the one presented here.

E. Cycle Slips Observed in Laboratory Testing

Another indicator of carrier tracking loop performance near threshold is the frequency of cycle slips. This parameter was not measured at Goldstone because of time limitation, but the effect was simulated in the laboratory at 4-dB carrier margin. Carrier arraying significantly reduced the frequency of cycle slips, as shown in Fig. 6.

V. Conclusions

The demonstration conducted at Goldstone in May 1990 showed that an antenna with an inadequate G/T can indeed track a weak signal by carrier arraying with another antenna and produce telemetry baseband. Baseband-combining techniques can then be used to achieve a higher telemetry signal-to-noise ratio.

This demonstration marked the first time that carrier arraying was tried in the DSN to receive a spacecraft signal. The full benefit of combined aperture of two antennas was realized by using carrier arraying and baseband combining together. Lessons learned in this demonstration are applicable to the design of the next generation of DSN receivers.

Optimal design of a carrier-arraying system should consider all sources of phase errors, including both thermal and phase noises. An analytical model is presented to allow such evaluation. Predictions based on this model agree well with the Pioneer 11 data received, except for baseband-combining gain in the 3-way mode. Further investigation is needed to characterize the effect of correlated phase noise on the efficiency of baseband combining.

Acknowledgments

The authors are indebted to Robertson Stevens of the Telecommunications and Data Acquisition Office, whose encouragement made this demonstration possible. They also thank Clarence Hoynes and Joseph Johnson for operational support at Goldstone, and Peter Kinman and Stan Butman for many helpful discussions.

References

[1] M. H. Brockman, "Radio Frequency Carrier Arraying for High Rate Telemetry Reception," *DSN Progress Report 42-45*, vol. March and April 1978, Jet Propulsion Laboratory, Pasadena, California, pp. 209–223, June 15, 1978.

[2] D. Divsalar and J. H. Yuen, "Improved Carrier Tracking Performance with Coupled Phase-Locked Loops," *TDA Progress Report 42-66*, vol. September and October 1981, Jet Propulsion Laboratory, Pasadena, California, pp. 148–171, December 15, 1981.

[3] M. H. Brockman, "Performance Characteristics for an Array of Two Receiving Systems with Equal Apertures and Enhanced Radio Frequency Carrier Margin Improvement," *TDA Progress Report 42-84*, vol. October–December 1985, Jet Propulsion Laboratory, Pasadena, California, pp. 112–126, February 15, 1986.

[4] R. Winkelstein, "Analysis of the Signal Combiner for Multiple Antenna Arraying," *Deep Space Network Progress Report 42-26*, Jet Propulsion Laboratory, Pasadena, California, pp. 102–118, January–February 1975.

[5] J. H. Yuen, ed., *Deep Space Telecommunications System Engineering*, JPL Publication 82-76, Jet Propulsion Laboratory, Pasadena, California, pp. 206–211, July 1982.

[6] V. A. Vilnrotter, W. J. Hurd, and D. H. Brown, "Optimized Tracking of RF Carriers With Phase Noise, Including Pioneer 10 Results," *TDA Progress Report 42-91*, vol. July–September 1987, Jet Propulsion Laboratory, Pasadena, California, pp. 141–157, November 15, 1987.

[7] R. Bunce, "Effect of VCO Noise on Phase-Lock Receiver," *JPL Space Programs Summary 37-61*, vol. 2, Jet Propulsion Laboratory, Pasadena, California, pp. 115–120, 1969.

Table 1. Pioneer 11 signal and noise conditions at Goldstone, 10-deg elevation, May 1990

Item	70-m, DSS 14	34-m STD, DSS 12	34-m HEF, DSS 15
P_c, dBm[a]	−167	−174	−174
T_{op}, K	30.5	33.5	47.5
N_0, dBm/Hz	−183.8	−183.3	−181.8
$2B_{L0}$, Hz	3	12[b]	12
Carrier margin[b] ($P_c/2N_0B_{L0}$), dB	12.0	−1.5[c]	−3.0

[a] Pioneer 10 signal level is about 5.5 dB lower than that of Pioneer 11.

[b] During the carrier arraying test, a 3-Hz bandwidth loop was used for DSS 12, with a carrier margin of 4.5 dB.

[c] Carrier margin for reliable signal acquisition and tracking should exceed 7 dB.

Table 2. Predicted DSS 12 receiver rms phase error, σ, contributed by various sources in the 1-way mode, rad

Source	Carrier not combined	Carrier combined
Thermal noise, DSS 12	0.53	0.29
Thermal noise, DSS 15	0	0.30
Phase noise, spacecraft	0.055	0.053
Phase noise, DSS 12 VCO	0.10	0.099
Phase noise, DSS 15 VCO	0	0.033
Total, rss	0.54	0.43
Symbol SNR degradation	−1.21 dB	−0.79 dB

Note: Spacecraft phase-noise effect would be 0.19 rad rms for the 3-way mode.

Table 3. Predicted DSS 15 receiver rms phase error, σ, contributed by various sources in the 1-way mode, rad

Source	Carrier not combined	Carrier combined
Thermal noise, DSS 12	0.51	0.52
Thermal noise, DSS 15	0.18	0.37
Phase noise, spacecraft	0.052	0.049
Phase noise, DSS 12 VCO	0.097	0.091
Phase noise, DSS 15 VCO	0.036	0.032
Total, rss	0.55	0.47
Symbol SNR degradation	−1.28 dB	−0.94 dB

Note: Spacecraft phase-noise effect would be 0.19 rad rms for the 3-way mode.

Table 4. Comparison between observed and predicted performance

Item	Observed	Predicted
Carrier-combining gain, dB		
1-way	0.31 ± 0.4	0.42
3-way	0.35 ± 0.5	0.40
Baseband-combining gain, dB		
1-way	2.15 ± 0.5	2.35
3-way	1.40 ± 0.5	2.35
Degradation from 1-way to 3-way, dB, DSS 12 or combined	−0.26 ± 0.5	−0.14
Laboratory test without Doppler or phase noise		
Carrier-combining gain, dB	1.27 ± 0.7	0.35
Baseband-combining gain, dB	2.10 ± 0.6	2.35

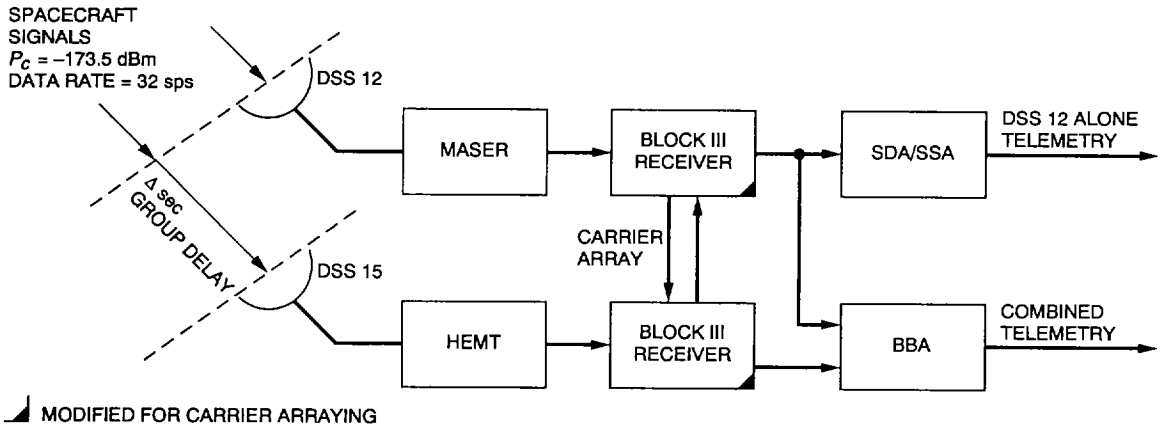

Fig. 1. Configuration of carrier-arraying demonstration.

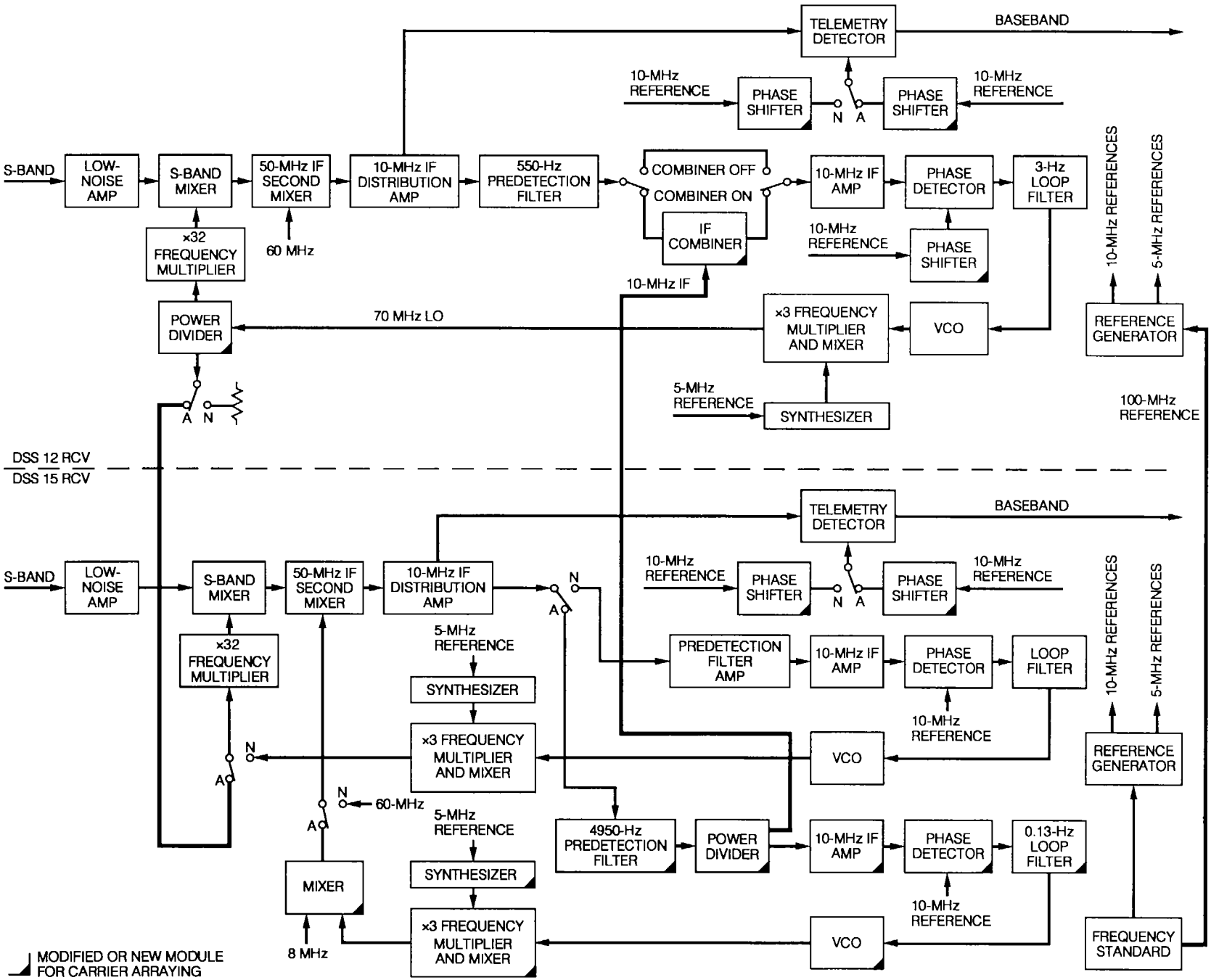

Fig. 2. Modifications of Block III receivers for carrier-arraying demonstration.

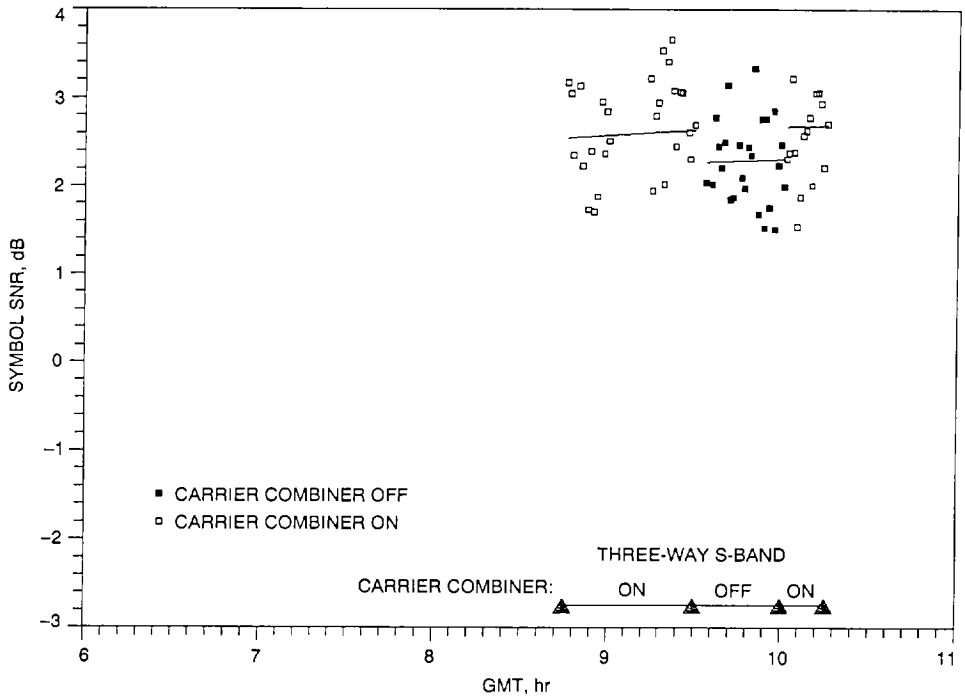

Fig. 3. Symbol SNR of combined telemetry on May 3, 1990.

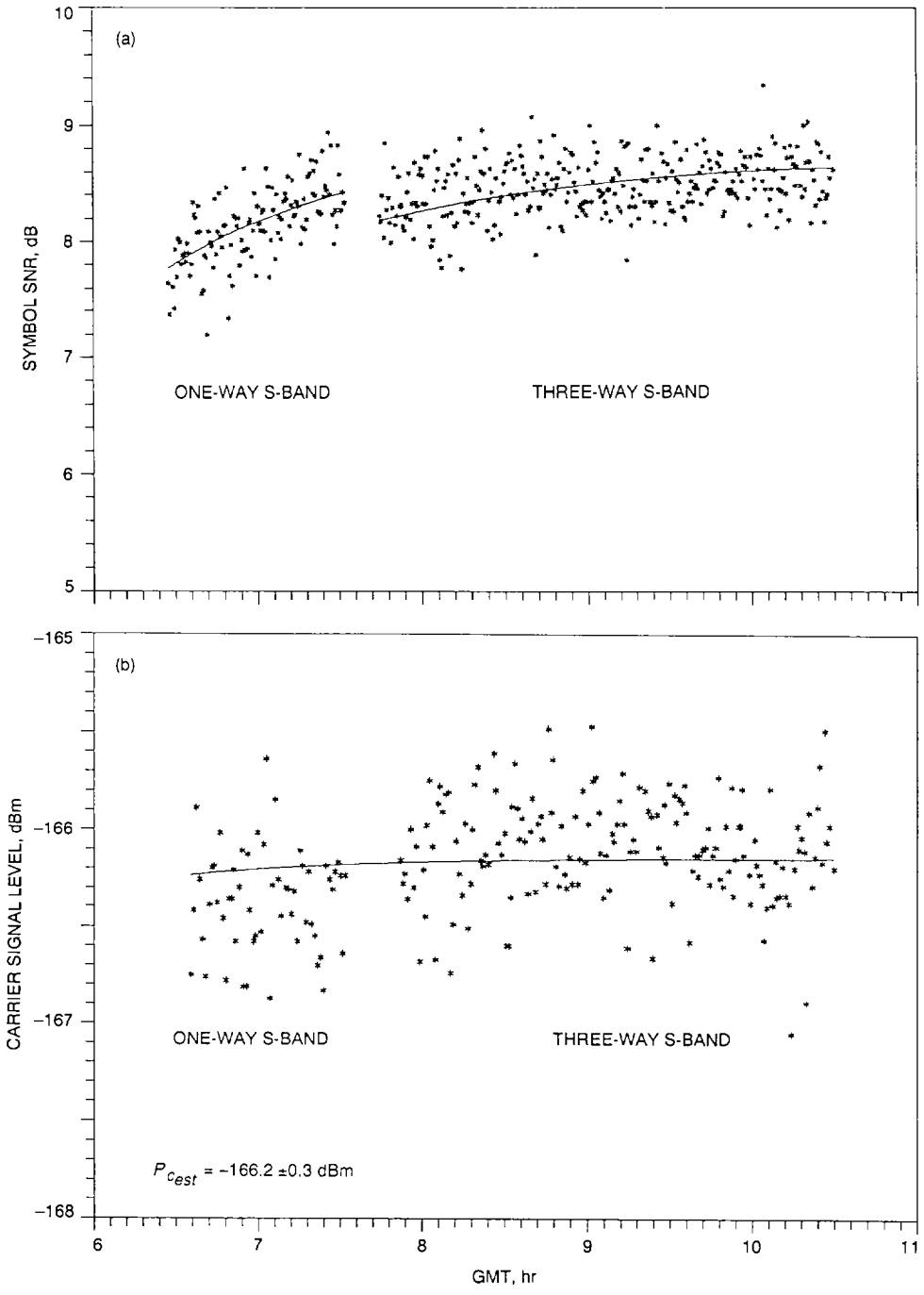

Fig. 4. May 3, 1990 DSS 14 measurements during Pioneer 11 track: (a) symbol SNR, and (b) carrier signal level.

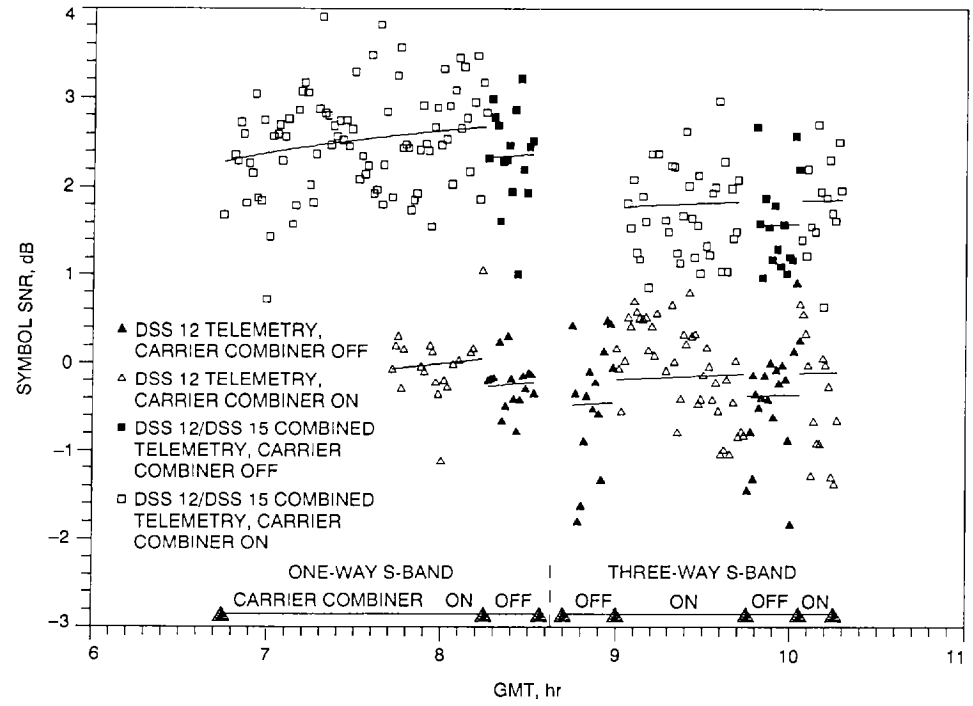

Fig. 5. Symbol SNR of single and combined telemetry on May 6, 1990.

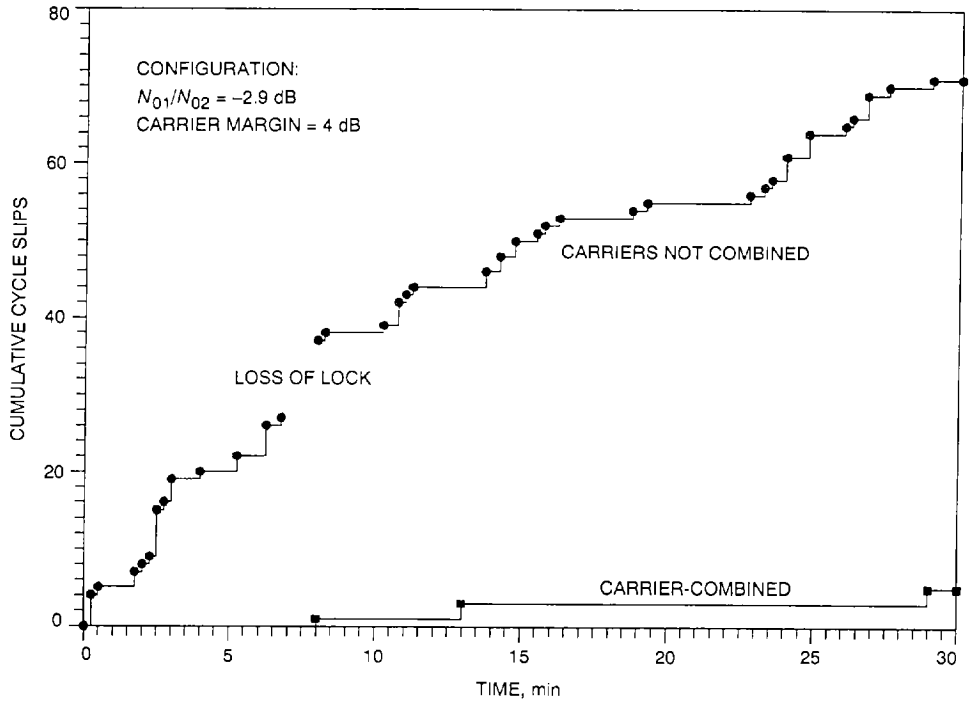

Fig. 6. Cycle slips measured in the laboratory on March 20, 1990.

Appendix A

The Effects of Spacecraft and Ground Receiver VCO Phase Noise on the Performance of Carrier-Arrayed Receivers

Consider the carrier-arraying system illustrated in Fig. A-1, its mathematical equivalent in Fig. A-2, and the equivalent with phase-noise effects in Fig. A-3. (These figures are taken directly from [2] where station and oscillator phase noise was not accounted for.) Assume now that each of the voltage-controlled oscillators (VCOs) has an associated phase noise, namely $\psi_{R_i}(t)$; $i = 1, 2, \ldots, N$. Then the instantaneous frequency $\dot{\theta}(t)$ of the ith VCO output, referenced to zero, is now related to the ith VCO input $z_i(t)$ by

$$\dot{\hat{\theta}}_i(t) = K_{VCO_i} z_i(t) + \dot{\psi}_{R_i}(t) \tag{A-1}$$

where a dot over a variable denotes differentiation with respect to time and K_{VCO_i} denotes the gain of the ith VCO. Letting p denote the Heaviside operator, that is, $px = dx/dt$, then in terms of the ith loop filter input $\tilde{S}_i(t)$, Eq. (A-1) can be rewritten as

$$\hat{\theta}_i(t) = \frac{K_{VCO_i}}{p}\left[F_i(p)\tilde{S}_i\right] + \psi_{R_i} \tag{A-2}$$

By expressing $\tilde{S}_i(t)$ in terms of the parameters characterizing the various loop input signals, then analogous to Eq. (A-1) in [2], the estimated carrier phase at the output of the VCO of station 1 is now

$$\hat{\theta}_1 = \frac{K_1 F_1(p)}{p}\left[\sqrt{P_1}\cos\theta_m \sin\left(\theta_1 + \psi_{T_1} - \hat{\theta}_1\right) + \sum_{i=2}^{N}\sqrt{P_i}\beta_i \cos\theta_m \sin\left(\theta_i + \psi_{T_i} - \hat{\theta}_i - \hat{\theta}_1\right) + \sum_{i=1}^{N}\beta_i N_i\right] + \psi_{R_1} \tag{A-3}$$

where

θ_i = the carrier phase at station i; $i = 1, 2, \ldots, N$

ψ_{T_i} = the phase noise of the spacecraft signal received at station i; $i = 1, 2, \ldots, N$

β_i = the weight associated with the signal from station i at the input to the carrier combiner; $\beta_1 = 1$

θ_m = the modulation index

N_i = a Gaussian noise process with one-sided power spectral density N_{0i}; $i = 1, 2, \ldots, N$

K_i = the total gain in the ith loop

Assume now that the time delay between the various stations is small as compared with the reciprocal of the bandwidth of the phase-noise process associated with the spacecraft signal. Then $\psi_{T_i} = \psi_T$ can be set for all $i = 1, 2, \ldots, N$. If the loop at station 1 is now linearized (i.e., assume that $\sin x = x$), then Eq. (A-3) simplifies to

$$\hat{\theta}_1 = \frac{K_1 F_1(p)}{p}\left[\left(\sqrt{P_1}\cos\theta_m\right)\left(\theta_1 + \psi_T - \hat{\theta}_1\right) + \sum_{i=2}^{N}\left(\sqrt{P_i}\beta_i\cos\theta_m\right)\left(\theta_i + \psi_T - \hat{\theta}_i - \hat{\theta}_1\right) + \sum_{i=1}^{N}\beta_i N_i\right] + \psi_{R_1} \tag{A-4}$$

Similarly, for station i; $i = 2, \ldots, N$ (after linearization),

$$\hat{\theta}_i = \frac{K_i F_i(p)}{p}\left[\left(\sqrt{P_i}\cos\theta_m\right)(\theta_i + \psi_T - \hat{\theta}_i - \hat{\theta}_1) + N_i\right] + \psi_{R_i} \tag{A-5}$$

Solving for $\hat{\theta}_i$ in Eq. (A-5) yields

$$\hat{\theta}_i = H_i(p)\left[(\theta_i + \psi_T - \hat{\theta}_1) + \frac{N_i}{\sqrt{P_i}\cos\theta_m}\right] + [1 - H_i(p)]\psi_{R_i}; \quad i = 2, 3, \ldots, N \tag{A-6}$$

where $H_i(p)$ is a closed-loop transfer function defined by

$$H_i(p) = \frac{K_i F_i(p)\sqrt{P_i}\cos\theta_m}{p + K_i F_i(p)\sqrt{P_i}\cos\theta_m}; \quad i = 1, 2, \ldots, N \tag{A-7}$$

Substituting Eq. (A-6) into Eq. (A-4) gives

$$\hat{\theta}_1 = H_1(p)\left[\theta_1 + \psi_T + \frac{N_1}{\sqrt{P_1}\cos\theta_m} + \sum_{i=2}^{N}\beta_i\gamma_i[1 - H_i(p)]\left(\theta_i + \psi_T - \hat{\theta}_1 + \frac{N_i}{\sqrt{P_i}\cos\theta_m} - \psi_{R_i}\right)\right] + [1 - H_1(p)]\psi_{R_1} \tag{A-8}$$

where $\gamma_i = \sqrt{P_i/P_1}$. Finally, letting $\Delta\psi_i = \psi_T - \psi_{R_i}$ represent the differential phase noise for the ith station and then solving Eq. (A-8) for $\hat{\theta}_1$,

$$\hat{\theta}_1 = \frac{H_1(p)\left[\theta_1 + \psi_T + \frac{N_1}{\sqrt{P_1}\cos\theta_m} + \sum_{i=2}^{N}\beta_i\gamma_i[1 - H_i(p)]\left(\theta_i + \frac{N_i}{\sqrt{P_i}\cos\theta_m} + \Delta\psi_i\right)\right]}{1 + \sum_{i=2}^{N}\beta_i\gamma_i H_1(p)[1 - H_i(p)]}$$

$$+ \frac{[1 - H_1(p)]\psi_{R_1}}{1 + \sum_{i=2}^{N}\beta_i\gamma_i H_1(p)[1 - H_i(p)]} \tag{A-9}$$

By comparing Eq. (A-9) with Eq. (A-7) in [2], Fig. A-2 can be immediately redrawn to include the effects of phase noise. The resulting equivalent linearized representation is illustrated in Fig. A-3.

Now the phase error in loop 1 is given by

$$\phi_1 = \theta_1 + \psi_T - \hat{\theta}_1 \tag{A-10}$$

Substituting Eq. (A-10) into Eq. (A-9) and simplifying gives the desired result:

$$\phi_1 = \frac{1 - H_1(p) + \sum_{i=2}^{N} \beta_i \gamma_i H_1(p)[1 - H_i(p)]}{1 + \sum_{i=2}^{N} \beta_i \gamma_i H_1(p)[1 - H_i(p)]} \theta_1 + \frac{1 - H_1(p)}{1 + \sum_{i=2}^{N} \beta_i \gamma_i H_1(p)[1 - H_i(p)]} \Delta\psi_1$$

$$- \frac{H_1(p)}{1 + \sum_{i=2}^{N} \beta_i \gamma_i H_1(p)[1 - H_i(p)]} \left[\frac{N_1}{\sqrt{P_1} \cos\theta_m} + \sum_{i=2}^{N} \beta_i \gamma_i [1 - H_i(p)] \left(\theta_i + \frac{N_i}{\sqrt{P_i} \cos\theta_m} - \psi_{R_i} \right) \right] \tag{A-11}$$

The mean-square phase jitter evaluation is provided below. The mean-square phase jitter in loop i; $i = 1, 2, \ldots, N$, is defined by

$$\sigma^2_{\phi_i} = E\Big\{ [\phi_i(s) - E\{\phi_i(s)\}] [\phi_i(-s) - E\{\phi_i(-s)\}] \Big\} \tag{A-12}$$

where E denotes statistical expectation and s is the Laplace transform operator. By using Eq. (A-11) in Eq. (A-12), one obtains for loop 1

$$\sigma^2_{\phi_1} = \frac{1}{2\pi j} \int \left| \frac{H_1(s)}{1 + \sum_{i=2}^{N} \beta_i \gamma_i H_1(s)[1 - H_i(s)]} \right|^2 ds \frac{N_{01}}{2P_1 \cos^2\theta_m}$$

$$+ \sum_{i=2}^{N} \beta_i^2 \gamma_i^2 \frac{1}{2\pi j} \int \left| \frac{H_1(s)[1 - H_i(s)]}{1 + \sum_{i=2}^{N} \beta_i \gamma_i H_1(s)[1 - H_i(s)]} \right|^2 ds \frac{N_{0i}}{2P_i \cos^2\theta_m}$$

$$+ \frac{1}{2\pi j} \int \left| \frac{1 - H_1(s)}{1 + \sum_{i=2}^{N} \beta_i \gamma_i H_1(s)[1 - H_i(s)]} \right|^2 S_{\Delta\psi_1}(s)\, ds + \sum_{i=2}^{N} \beta_i^2 \gamma_i^2 \frac{1}{2\pi j} \int \left| \frac{H_1(s)[1 - H_i(s)]}{1 + \sum_{i=2}^{N} \beta_i \gamma_i H_1(s)[1 - H_i(s)]} \right|^2 S_{\psi_{R_i}}(s)\, ds \tag{A-13}$$

where

$$\left.\begin{aligned} S_{\psi_{T_i}}(s) &= E\{\psi_{T_i}(s)\psi_{T_i}(-s)\} \\ S_{\psi_{R_i}}(s) &= E\{\psi_{R_i}(s)\psi_{R_i}(-s)\} \\ S_{\Delta\psi_i}(s) &= S_{\psi_{T_i}}(s) + S_{\psi_{R_i}}(s) \end{aligned}\right\} \tag{A-14}$$

are the two-sided power spectral densities associated with the phase-noise processes. In arriving at the third equation of Eq. (A-14), it has also been assumed that the transmit and receive phase-noise processes are uncorrelated. The first two terms of Eq. (A-13) are identical to Eq. (16) in [2]; the remaining two terms reflect the added degradation due to the various spacecraft and VCO phase-noise sources.

Under the assumption $H_i(s) = H_2(s)$; $i = 3, 4 \ldots, N$, Eq. (A-13) simplifies to

$$\sigma^2_{\phi_1} = \frac{1}{2\pi j}\int \left|\frac{H_1(s)}{1 + H_1(s)[1 - H_2(s)](G-1)}\right|^2 ds \frac{N_{01}}{2P_1 \cos^2\theta_m}$$

$$+ \sum_{i=2}^{N} \beta_i^2 \gamma_i^2 \frac{1}{2\pi j}\int \left|\frac{H_1(s)[1 - H_2(s)]}{1 + H_1(s)[1 - H_2(s)](G-1)}\right|^2 ds \frac{N_{0i}}{2P_i \cos^2\theta_m}$$

$$+ \frac{1}{2\pi j}\int \left|\frac{1 - H_1(s)}{1 + H_1(s)[1 - H_2(s)](G-1)}\right|^2 S_{\Delta\psi_1}(s) ds + \sum_{i=2}^{N} \beta_i^2 \gamma_i^2 \frac{1}{2\pi j}\int \left|\frac{H_1(s)[1 - H_2(s)]}{1 + H_1(s)[1 - H_2(s)](G-1)}\right|^2 S_{\psi_{R_i}}(s)\, ds \tag{A-15}$$

where

$$G = \sum_{i=1}^{N} \beta_i \gamma_i; \quad G - 1 = \sum_{i=2}^{N} \beta_i \gamma_i \tag{A-16}$$

The remaining step is to express Eq. (A-15) in terms of the loop dynamic parameters, such as damping and noise bandwidth. To do this, consider the case of second-order loops with imperfect integrating filters, i.e.,

$$F_i(s) = \frac{1 + \tau_{2i}(s)}{1 + \tau_{1i}(s)}; \quad \tau_{2i} << \tau_{1i} \tag{A-17}$$

Substituting Eq. (A-17) into Eq. (A-7) and recalling that the loop damping parameter r_i for the ith loop is defined by

$$r_i = \sqrt{P_i} \cos\theta_m K_i \tau_{2i}^2 / \tau_{1i} \tag{A-18}$$

one obtains

$$H_i(s) = \frac{r_i\left(\frac{1}{\tau_{2i}^2} + \frac{s}{\tau_{2i}}\right)}{s^2 + \frac{r_i}{\tau_{2i}}s + \frac{r_i}{\tau_{2i}^2}} = \frac{1 + \frac{r_i + 1}{4B_{Li}}s}{1 + \frac{r_i + 1}{4B_{Li}}s + \frac{1}{r_i}\left(\frac{r_i + 1}{4B_{Li}}\right)^2 s^2} \tag{A-19}$$

where B_{Li} denotes the loop noise bandwidth for the ith loop.

The phase error in loop i; $i = 2, 3, \ldots, N$, is given by

$$\phi_i = \theta_i + \psi_T - \hat{\theta}_1 - \hat{\theta}_i = \underbrace{\theta_1 + \psi_T - \hat{\theta}_1}_{\phi_1} + \underbrace{\theta_i - \theta_1 - \hat{\theta}_i}_{\phi_{ei}} \tag{A-20}$$

where ϕ_{ei} represents the phase error in loop i relative to that in loop 1. Using Eqs. (A-6)–(A-11), one obtains for loop i; $i = 2, 3, \ldots, N$,

$$\phi_i = (1 - H_i(p))\theta_i - D^{-1}H_1(p)(1 - H_i(p))\left(\theta_1 + \frac{N_1}{\sqrt{P_1}\cos\theta_m}\right)$$

$$- D^{-1}\left(H_i(p) + \beta_i\gamma_i H_1(p)(1 - H_i(p)) + H_i(p)\sum_{\substack{k=2\\k\neq i}}^{N}\beta_k\gamma_k H_1(p)(1 - H_i(p))\right)\left(\frac{N_i}{\sqrt{P_i}\cos\theta_m}\right)$$

$$- D^{-1}(1 - H_i(p))\sum_{\substack{k=2\\k\neq i}}^{N}\beta_k\gamma_k H_1(p)(1 - H_i(p))\left(\frac{N_k}{\sqrt{P_k}\cos\theta_m}\right) + D^{-1}(1 - H_i(p))(1 - H_1(p))\Delta\psi_1$$

$$- D^{-1}(1 - H_i(p))\left(1 + \sum_{\substack{k=2\\k\neq i}}^{N}\beta_k\gamma_k H_1(p)(1 - H_i(p))\right)\psi_{R_i} + D^{-1}(1 - H_i(p))\sum_{\substack{k=2\\k\neq i}}^{N}\beta_k\gamma_k H_1(p)(1 - H_i(p))\psi_{R_i} \tag{A-21}$$

where

$$D = 1 + \sum_{k=2}^{N}\beta_k\gamma_k H_1(p)(1 - H_i(p)) \tag{A-22}$$

Assuming again that $H_i(s) = H_2(s)$; $i = 3, 4, \ldots, N$, then analogous to Eq. (A-15), the total mean-squared phase error in loop i is

$$\sigma^2_{\phi_i} = \frac{1}{2\pi j}\int\left|\frac{H_1(s)[1 - H_2(s)]}{1 + H_1(s)[1 - H_2(s)](G - 1)}\right|^2 ds\frac{N_{01}}{2P_1\cos^2\theta_m}$$

$$+ \frac{1}{2\pi j}\int\left|1 - \frac{[1 - H_2(s)][1 + H_1(s)[1 - H_2(s)](G_i' - 1)]}{1 + H_1(s)[1 - H_2(s)](G - 1)}\right|^2 ds\frac{N_{0i}}{2P_i\cos^2\theta_m}$$

$$+ \sum_{\substack{k=2\\k\neq i}}^{N}\beta_k^2\gamma_k^2\frac{1}{2\pi j}\int\left|\frac{H_1(s)[1 - H_2(s)]^2}{1 + H_1(s)[1 - H_2(s)](G - 1)}\right|^2 ds\frac{N_{0k}}{2P_k\cos^2\theta_m} + \frac{1}{2\pi j}\int\left|\frac{[1 - H_1(s)][1 - H_2(s)]}{1 + H_1(s)[1 - H_2(s)](G - 1)}\right|^2 S_{\Delta\psi_1}(s)\,ds$$

$$+ \frac{1}{2\pi j}\int\left|\frac{[1 - H_2(s)][1 + H_1(s)[1 - H_2(s)](G_i' - 1)]}{1 + H_1(s)[1 - H_2(s)](G - 1)}\right|^2 S_{\psi_{R_i}}(s)\,ds$$

$$+ \sum_{\substack{k=2\\k\neq i}}^{N}\beta_k^2\gamma_k^2\frac{1}{2\pi j}\int\left|\frac{H_1(s)[1 - H_2(s)]^2}{1 + H_1(s)[1 - H_2(s)](G - 1)}\right|^2 S_{\psi_{Rk}}(s)\,ds \tag{A-23}$$

where G and $G - 1$ are as in Eq. (A-16), and in addition

$$G_i' - 1 = \sum_{\substack{k=2 \\ k \neq i}}^{N} \beta_k \gamma_k \tag{A-24}$$

For $N = 2$, Eq. (A-23) simplifies to

$$\sigma_{\phi_2}^2 = \frac{1}{2\pi j} \int \left| \frac{H_1(s)[1 - H_2(s)]}{1 + H_1(s)[1 - H_2(s)](G-1)} \right|^2 ds \frac{N_{01}}{2P_1 \cos^2 \theta_m}$$

$$+ \frac{1}{2\pi j} \int \left| \frac{H_1(s)[1 - H_2(s)](G-1) + H_2(s)}{1 + H_1(s)[1 - H_2(s)](G-1)} \right|^2 ds \frac{N_{02}}{2P_2 \cos^2 \theta_m}$$

$$+ \frac{1}{2\pi j} \int \left| \frac{[1 - H_1(s)][1 + H_2(s)]}{1 + H_1(s)[1 - H_2(s)](G-1)} \right|^2 S_{\Delta\psi_1}(s)\, ds + \frac{1}{2\pi j} \int \left| \frac{[1 - H_2(s)]}{1 + H_1(s)[1 - H_2(s)](G-1)} \right|^2 S_{\psi_{R2}}(s)\, ds \tag{A-25}$$

where now

$$G - 1 = \beta_2 \gamma_2 \tag{A-26}$$

Note that in the presence of the bandpass limiter in the receiver system, the limiter performance factor Γ, defined in Eq. (B-5) of Appendix B, should be included in the thermal contributions (first and second term) in Eqs. (A-15) and (A-25).

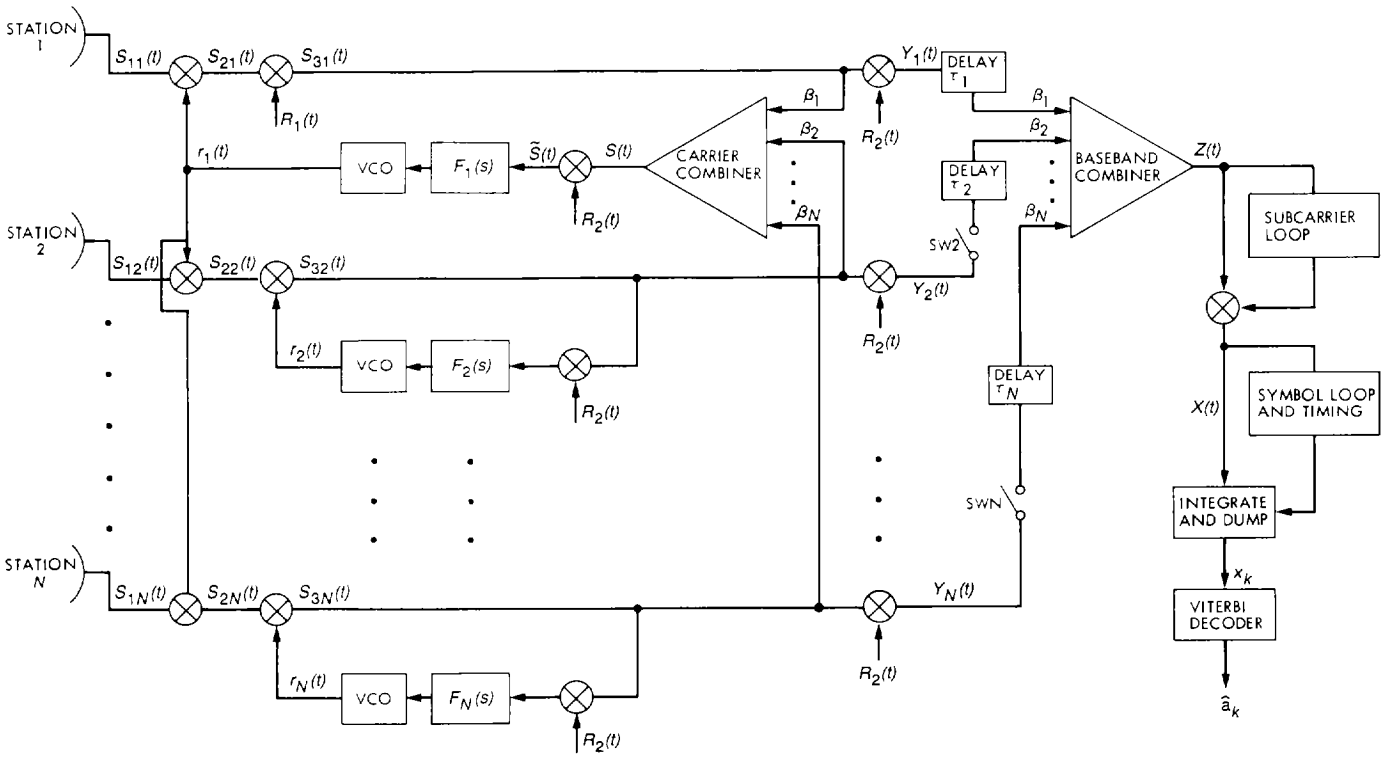

Fig. A-1. Configuration for arrayed network with carrier and baseband arraying.

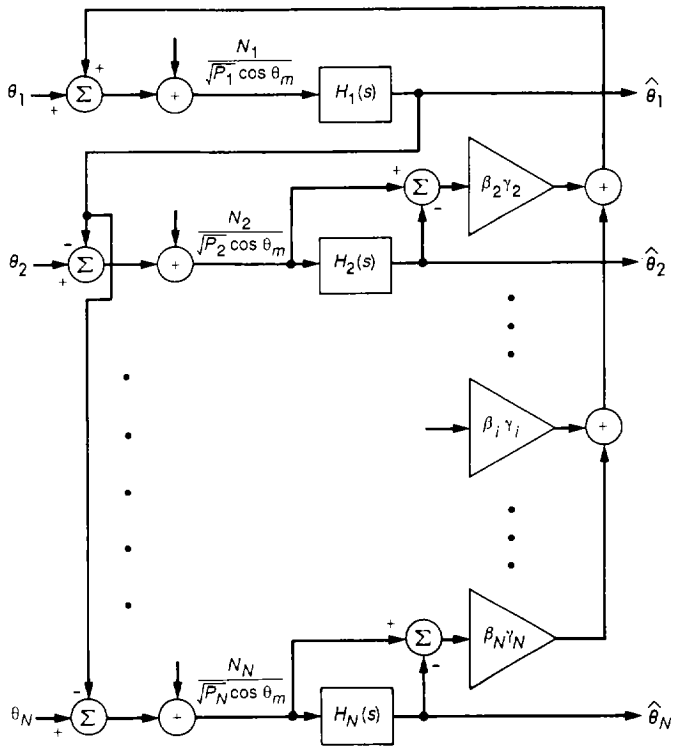

Fig. A-2. An equivalent linear representation of carrier-arraying system for phase jitter analysis.

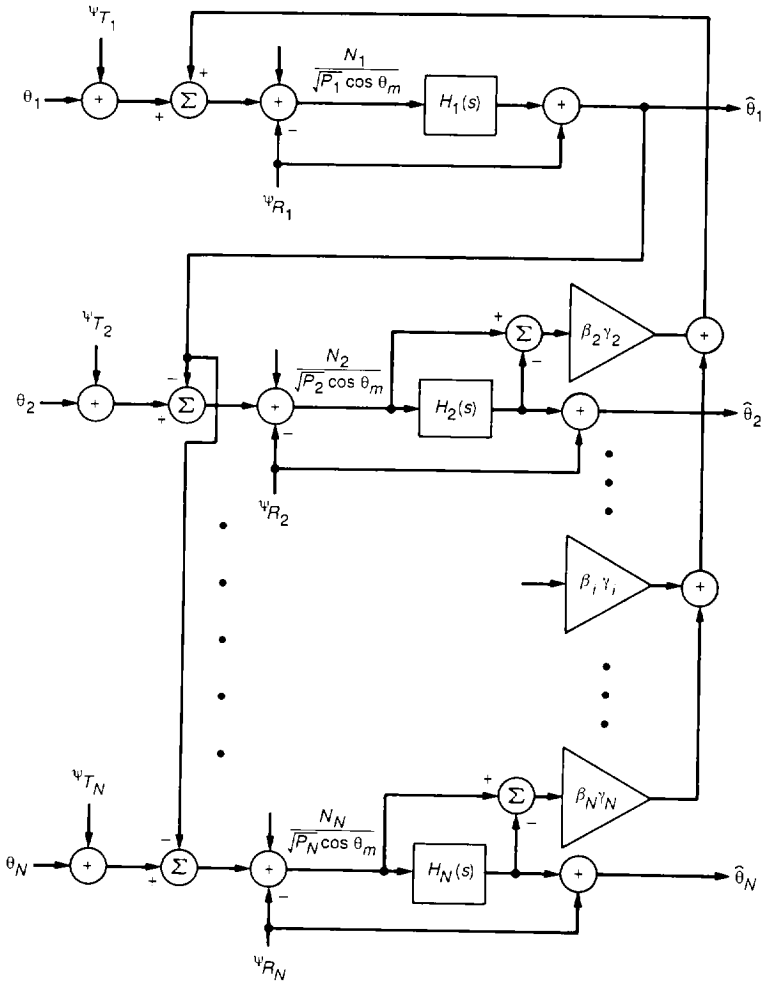

Fig. A-3. An equivalent linear representation of carrier-arraying system for phase jitter analysis (phase-noise effects included).

Appendix B

Optimum Design of Carrier-Arrayed Receivers With Different IF Filter Bandwidths

I. Background

A brief summary of the key results from [2], which is referenced later, is given here.

For $i = 1, 2, \ldots, N$, let β_i denote the weights applied to each signal entering the carrier combiner, P_{ci} denote the received carrier powers of the station input signals, B_{Li} denote the single-sided loop noise bandwidth of each receiver in the absence of arraying, and N_{0i} denote the noise power spectral densities of the receivers. Furthermore, for simplicity, assume that the loop gains and loop filters for stations $2, 3, \ldots, N$ are identical. This is tantamount to assuming that the receiver closed-loop transfer functipns, $H_i(s)$, $i = 2, 3, \ldots, N$ are identical, or equivalently that $H_i(s) = H_2(s)$ for $i = 3, 4, \ldots, N$. Then, in the presence of carrier arraying, the mean-squared phase jitter of receiver 1 (the aided station) is given by

$$\sigma_{\phi 1}^2 = \frac{B_L \sum_{i=1}^{N} \beta_i^2 N_{0i}}{G^2 P_{c1}} \tag{B-1}$$

where

$$G = \sum_{i=1}^{N} \beta_i \gamma_i = 1 + \sum_{i=2}^{N} \beta_i \gamma_i \; ; \quad \gamma_i = \sqrt{\frac{P_{ci}}{P_{c1}}} \tag{B-2}$$

is the array "gain" and B_L is the loop bandwidth of receiver 1 in the presence of arraying, which is related to the loop bandwidth of receiver 1 in the absence of arraying B_{L1} by

$$B_L = \frac{1 + Gr_1}{1 + r_1} B_{L1} = \frac{1 + r}{1 + r_1} B_{L1} \tag{B-3}$$

Here, r_1 is the loop-damping parameter of receiver 1 in the absence of arraying, and $r = Gr_1$ is the same parameter in the presence of carrier arraying.

Consider now the effect of a bandpass limiter preceding each loop with IF bandwidths B_{IF_i}; $i = 1, 2, \ldots, N$. Equation (B-1) then becomes

$$\sigma_{\phi 1}^2 = \frac{\tilde{B}_L \Gamma \sum_{i=1}^{N} \beta_i^2 N_{0i}}{G^2 P_{c1}} \tag{B-4}$$

where Γ is the limiter performance factor approximately given by

$$\Gamma \cong \frac{1 + \rho_{in}}{0.862 + \rho_{in}} \tag{B-5}$$

and $\tilde{B}_L$ is the loop bandwidth with carrier arraying, which is given by

$$\tilde{B}_L = \frac{1 + \tilde{r}}{1 + r_1} B_{L1} \tag{B-6}$$

Here, ρ_{in} is the input SNR to the bandpass limiter of station 1, namely

$$\rho_{in} = \frac{G^2 P_{c1}}{\sum_{i=1}^{N} \beta_i^2 N_{0i} B_{IF_i}} \tag{B-7}$$

and $\tilde{r}$ is the loop damping of receiver 1 with carrier arraying, which is now given by

$$\tilde{r} = \frac{\sqrt{8/\pi^2}\,\tilde{\alpha}}{\sqrt{P_{c1}}} r_1 \tag{B-8}$$

with $\tilde{\alpha}$, the limiter suppression factor, approximated by

$$\tilde{\alpha} \cong \sqrt{\frac{0.7854\rho_{in} + 0.4768\rho_{in}^2}{1 + 1.024\rho_{in} + 0.4768\rho_{in}^2}} \tag{B-9}$$

Once the station receiver parameters have been defined for the unarrayed configuration, the mean-squared phase jitter of the arrayed system, as given in Eq. (B-4), can be minimized by proper selection of the combiner weights β_i; $i = 2, 3, \ldots, N$. The procedure for accomplishing this is discussed below. Note that the results described here differ from those discussed in [2] where it was assumed that

all IF filters had the same bandwidth. In the latter case it is possible to obtain an analytical characterization of the optimum weights, see Eq. (32) of [2]. Unfortunately, in the case of unequal IF filter bandwidths (e.g., the DSS 12 receiver has an IF bandwidth of 550 Hz whereas that of the DSS 15 receiver is 4950 Hz), it is not possible to analytically perform the optimization since the effective loop SNR is no longer a monotone increasing function of ρ_{in} as was assumed in [2].

II. Analysis

Without going through the details here, it was shown in [2] that when a bandpass limiter precedes the loop in each station (not indicated in Fig. 1), then the effective loop SNR, ρ_{L1}, of station 1 is given as the reciprocal of Eq. (B-4), namely,

$$\rho_{L1} = \frac{P_{c1}G^2}{\Gamma_1 \tilde{B}_{L1} \sum_{i=1}^{N} \beta_i^2 N_{0i}} \tag{B-10}$$

with Γ, $\tilde{B}_L$, ρ_{in}, and $\tilde{r}$ defined in Eqs. (B-5)–(B-8). These same parameters can be related to their values at threshold as follows. Letting the subscript "0" on a parameter denote its value at threshold, and defining the threshold condition (carrier arraying is assumed to be absent) by

$$\frac{P_{c10}}{2N_{01}\tilde{B}_{L0}} = 1 \tag{B-11}$$

then from Eq. (B-7), with $N = 1$ and $G = 1$,

$$\left.\begin{aligned} \rho_{in_{10}} &= \frac{P_{c10}}{N_{01}B_{IF_1}} = 2\frac{\tilde{B}_{L0}}{B_{IF_1}} \\ \tilde{\alpha}_0 &= \sqrt{\frac{0.785\rho_{in_{10}} + 0.4768\rho_{in_{10}}^2}{1 + 1.024\rho_{in_{10}} + 0.4768\rho_{in_{10}}^2}} \\ &\cong \sqrt{0.785\rho_{in_{10}}} \\ \tilde{B}_L &= \tilde{B}_{L0}\frac{1 + \tilde{r}_0\frac{\tilde{\alpha}}{\tilde{\alpha}_0}}{1 + \tilde{r}_0} \end{aligned}\right\} \tag{B-12}$$

Here, $\tilde{B}_{L0}$ and $\tilde{r}_0$ are, respectively, the values of loop bandwidth and damping factor associated with receiver 1 at threshold (no carrier arraying) and are specified in a given design, e.g., for DSS 12, $\tilde{B}_{L0} = 1.5$ Hz and $\tilde{r}_0 = 4$.

Since the radio loss associated with the data detection process is minimized by maximizing the loop SNR of the aided station, Eq. (B-10), one should select the set of weights $\{\beta_i;\ i = 2, 3, \ldots, N\}$ to achieve this goal. If the IF bandwidths of the receivers were all equal (as assumed in [2]), i.e., $B_{IF_i} = B_{IF}$ for all i, then one can find an analytical expression for these weights. The technique for doing this depends on recognizing that, for this case, ρ_{L1} is a monotonic increasing function of ρ_{in_1}; thus, maximizing ρ_{L1} with respect to the set of β_i's is equivalent to maximizing ρ_{in_1} with respect to the same parameters. When this is done, the following optimum set of weights results:

$$\beta_i = \gamma_i \frac{N_{01}}{N_{0i}}; \quad i = 2, 3, \ldots, N \tag{B-13}$$

While in principle, this same optimization can be accomplished for the case where the IF filter bandwidths are different, finding an analytical expression for the optimum weights is difficult. One reason is that ρ_{L1} is no longer a monotonic increasing function of ρ_{in_1} and thus one must directly maximize ρ_{L1} with respect to the set of β_i's.

To slightly simplify matters, consider the DSS 12/DSS 15 case where only two stations are involved, i.e., $N = 2$. Under these circumstances, Eq. (B-10) becomes

$$\rho_{L1} = \frac{P_{c1}}{\Gamma_1 N_{01}}\left[\frac{(1+\beta_2\gamma_2)^2}{1+\beta_2^2 K_{N2}}\right]\left(\frac{1+\tilde{r}_0}{\tilde{B}_{L0}}\right) \times \left(1 + \tilde{r}_0\sqrt{\left(\frac{P_{c1}}{2N_{01}\tilde{B}_{L0}}\right)\left[\frac{(1+\beta_2\gamma_2)^2}{1+\beta_2^2 K_2 K_{N2}}\right]}\right)^{-1} \tag{B-14}$$

where

$$K_{N2} = \frac{N_{02}}{N_{01}}; \quad K_2 = \frac{B_{IF_2}}{B_{IF_1}} \tag{B-15}$$

Differentiating Eq. (B-14) with respect to β_2, keeping in mind that Γ is also a function of β_2 through ρ_{in_1}, see Eqs. (B-5) and (B-7), and equating the result to zero gives the optimum value of β_2. Finding the analytical solution for this optimum β_2 is difficult. One can simplify matters somewhat by noting that for small ρ_{in_1} (as is typically the case of interest), Γ_1 can be replaced by its value at

$\rho_{in_1} = 0$, namely $\Gamma_{10} = 1/0.862 = 1.16$. Secondly, when γ_2 is not too small, the term involving the square root in Eq. (B-14) will be reasonably large as compared with unity. Making these approximations, Eq. (B-14) simplifies to

$$\rho_{L1} = \frac{P_{c1}}{\Gamma_0 N_{01}} \left(\frac{1+\tilde{r}_0}{\tilde{B}_{L0}}\right) \left(\tilde{r}_0 \sqrt{\left(\frac{P_{c1}}{2N_{01}\tilde{B}_{L0}}\right)}\right)^{-1}$$

$$\times \left[\frac{(1+\beta_2\gamma_2)}{1+\beta_2^2 K_{N2}} \sqrt{1+\beta_2^2 K_2 K_{N2}}\right]$$

$$= C\left[\frac{(1+\beta_2\gamma_2)}{1+\beta_2^2 K_{N2}} \sqrt{1+\beta_2^2 K_2 K_{N2}}\right] \qquad \text{(B-16)}$$

where C is a constant that is independent of β_2. Thus, the optimum value of β_2 can be approximately obtained by maximizing the quantity

$$I = \left[\frac{(1+\beta_2\gamma_2)^2(1+\beta_2^2 K_2 K_{N2})}{(1+\beta_2^2 K_{N2})^2}\right] \qquad \text{(B-17)}$$

with respect to β_2. Before giving this result, note that if $K_2 = 1$ (i.e., equal IF bandwidths), then Eq. (B-17) reduces to

$$I = \left[\frac{(1+\beta_2\gamma_2)^2}{(1+\beta_2^2 K_{N2})}\right] \qquad \text{(B-18)}$$

which, when maximized with respect to β_2, yields the solution in Eq. (B-13), i.e., $\beta_2 = \gamma_2/K_{N2}$.

Returning now to Eq. (B-17) with $K_2 \neq 1$, then differentiating with respect to β_2 and setting the result equal to zero gives the solution

$$\beta_2^3 K_2 K_{N2}^2 - \beta_2^2 \gamma_2 K_{N2}(2K_2 - 1)$$

$$- \beta_2 K_{N2}(K_2 - 1) - \gamma_2 = 0 \qquad \text{(B-19)}$$

For the DSS 12/DSS 15 case, $B_{IF_1} = 550$ Hz and $B_{IF_2} = 4950$ Hz. Thus, $K_2 = 9$ and Eq. (B-19) becomes

$$9\beta_2^3 K_{N2}^2 - 17\beta_2^2 \gamma_2 K_{N2} - 8\beta_2 K_{N2} - \gamma_2 = 0 \qquad \text{(B-20)}$$

The table below evaluates the optimum β_2, as determined from Eq. (B-20), for various values of $\gamma_2^2 = P_{c2}/P_{c1}$ and $K_{N2} = 1$.

γ_2^2	β_2
1	2.256
0.5	1.793
0.1	1.245

Note that these optimum values of β_2 exceed unity, which was the value assumed in [2].

To determine the sensitivity of the receiver performance to the optimum choice of β_2, examine a plot of ρ_{L1} versus β_2 for a fixed set of system parameters. These parameters are usually determined for a given carrier margin M, which is defined as the operating signal-to-noise ratio in the threshold loop bandwidth with no arraying, namely,

$$M = \frac{P_{c1}}{2N_{01}B_{L0}} \qquad \text{(B-21)}$$

which, in view of Eq. (B-11), becomes

$$M = \frac{P_{c1}}{P_{c10}} \qquad \text{(B-22)}$$

i.e., the ratio of the operating carrier power to its threshold value. Using Eq. (B-12) in Eq. (B-14), the loop SNR of station 1, ρ_{L1}, can be written in terms of M as

$$\rho_{L1} = \frac{2M}{\Gamma_1}\left[\frac{(1+\beta_2\gamma_2)^2}{1+\beta_2^2 K_{N2}}\right](1+\tilde{r}_0)$$

$$\times \left(1+\tilde{r}_0\sqrt{M\left[\frac{(1+\beta_2\gamma_2)^2}{1+\beta_2^2 K_2 K_{N2}}\right]}\right)^{-1} \qquad \text{(B-23)}$$

where the value of ρ_{in_1} needed in Eq. (B-5) to compute Γ_1 is given in terms of M by

$$\rho_{in_1} = \left(M\frac{2\tilde{B}_{L0}}{B_{IF_1}}\right)\left[\frac{(1+\beta_2\gamma_2)^2}{1+\beta_2^2 K_2 K_{N2}}\right] \qquad \text{(B-24)}$$

Figure B-1 is a plot of ρ_{L1} versus β_2 for three values of carrier margin and the following parameters:

$\tilde{B}_{LO} = 1.5$ Hz

$r_0 = 4$

$B_{IF_1} = 550$ Hz and $B_{IF_2} = 4950$ Hz

$k =$ Boltzmann constant (1.38×10^{-23} W/Hz-K)

$T_1 = 25.6$ K and $T_2 = 25.6$ K

$$K_{N2} = \frac{N_{02}}{N_{01}} = \frac{kT_2}{kT_1} = 1$$

$$K_2 = \frac{B_{IF_2}}{B_{IF_1}} = 9$$

$$\gamma_2^2 = \frac{P_{c2}}{P_{c1}} = 1$$

Figure B-2 is a similar plot for a set of parameters typical of the current DSS 12/DSS 15 design at a 30-deg elevation angle:

$\tilde{B}_{LO} = 1.5$ Hz

$\tilde{r}_0 = 4$

$B_{IF_1} = 550$ Hz and $B_{IF_2} = 4950$ Hz

$k =$ Boltzmann constant (1.38×10^{-23} W/Hz-K)

$T_1 = 30.6$ K and $T_2 = 41.5$ K

$$K_{N2} = \frac{N_{02}}{N_{01}} = \frac{kT_2}{kT_1} = 1.356$$

$$K_2 = \frac{B_{IF_2}}{B_{IF_1}} = 9$$

$$\gamma_2^2 = \frac{P_{c2}}{P_{c1}} = 1$$

Tabulated below are the optimum values of β_2 and the corresponding maximum values of ρ_{L1} as determined from Figs. B-1 and B-2, respectively. Also included for comparison are the values of ρ_{L1} corresponding to $\beta_2 = 1$.

From Fig. B-1:

M	β_2	ρ_{L1}
7.7 dB	1.0	14.36
	1.9	15.92
5.7 dB	1.0	10.99
	1.85	12.10
3.7 dB	1.0	8.35
	1.8	9.13

From Fig. B-2:

M	β_2	ρ_{L1}
7.0 dB	1.0	12.35
	1.45	12.79
5.0 dB	1.0	9.39
	1.4	9.68
3.0 dB	1.0	7.08
	1.35	7.26

Thus, for the above two examples, it is possible to gain as much as a 0.5-dB improvement in loop SNR by an optimum choice of β_2.

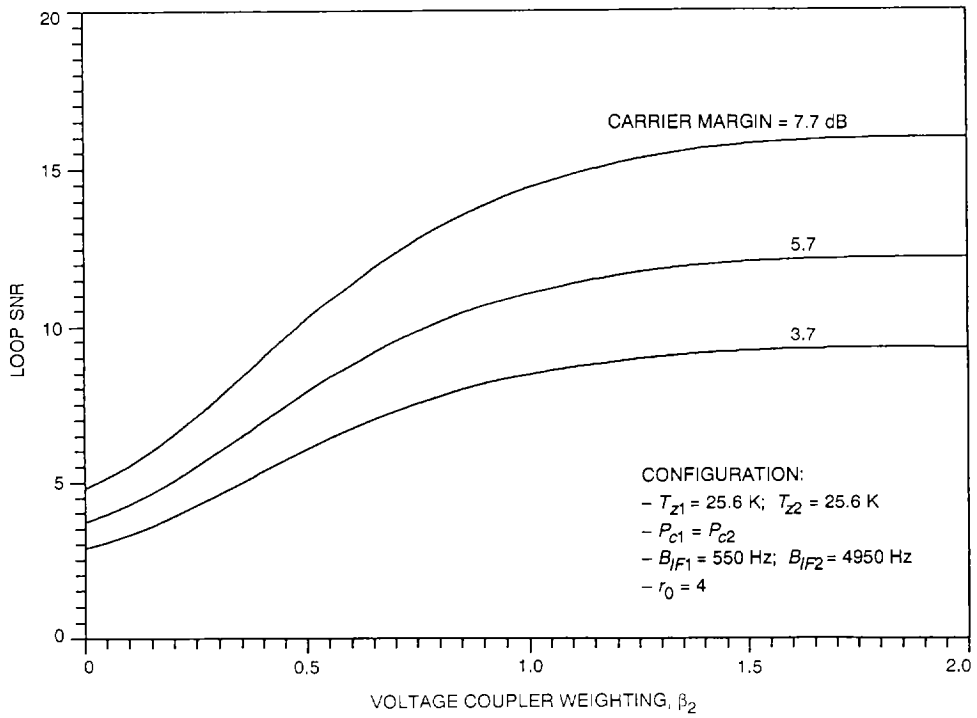

Fig. B-1. Loop SNR ρ_{L1} as a function of β and carrier margin.

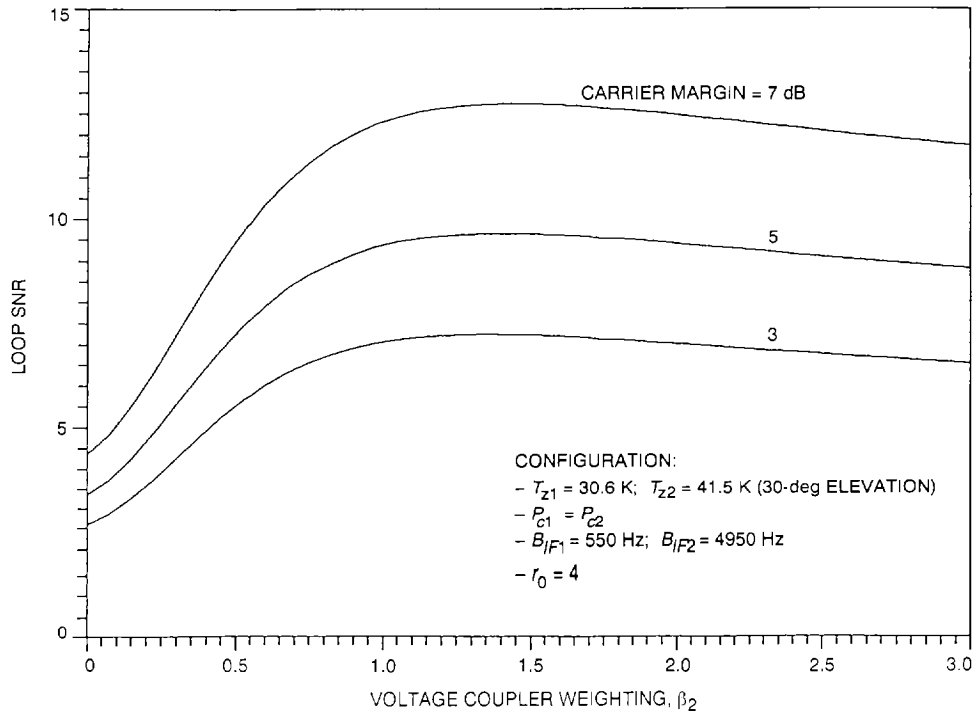

Fig. B-2. Loop SNR ρ_{L1} as a function of β and carrier margin, typical DSS 12/DSS 15 design at a 30-deg elevation angle.